Supplementary Information

A flexible silver-nanoparticle/polyacrylonitrile biomimetic strain sensor by patterned UV reduction for artificial intelligence flexible electronics

Jiaxiang Lu[1], Liang Su[1], Zhili Zhang[2], Wei Song[1], Shuang Hu[1], Jinbo Wang[1], Xilin Li[1], Yiping Huang[1], Zhaofeng He[2], Ming Lei[3*], Sen Lin[1,4*]

[1]School of Physical Science and Technology, Guangxi University, Nanning 530004, China.

[2]School of Artificial Intelligence, Beijing University of Posts and Telecommunications, Beijing 100876, China

[3]School of Integrated Circuits, Beijing University of Posts and Telecommunications, Beijing 100876, China

[4]Advanced Institute for Brain and Intelligence, Guangxi University, Nanning 530004, China.

This file includes:

Supplementary Methods

Supplementary Fig. S1-S30

Supplementary Table S1

Supplementary Video S1-S3

Supplementary References 1-9

Supplementary Methods

Materials and chemicals

Polyacrylonitrile (PAN, Mw=150 000), N,N-Dimethylformamide (DMF, >99.8%) were purchased from Shanghai Macklin Bio-Chem Technology Co. Ltd. Silver nitrate ($AgNO_3$) was purchased from Sinopharm Chemical Reagent Co., Ltd. Styrene Ethylene Butylene Styrene (SEBS) and Tetrahydrofuran (THF, >99%) were purchased from Shanghai Aladdin Bio-Chem Technology Co. Ltd. All reagents were used without further purification.

Preparation of the SPBSS

The precursor solution was prepared via the following procedures. First, 0.5g PAN was dissolved in 6g DMF and magnetically stirred at 70° C for 1 h. 3g $AgNO_3$ was add to the PAN solution. The mixed solution was magnetically stirred at ambient temperature for at least 2 h magnetically, yielding faint yellow transparent solution for preparing SPBSS.

The precursor solution was cast into the heat-resistant square container uniformly (The area of the square container is 3cm×3cm), and turn on the ultraviolet lamp and preheat for at least 15min to ensure sufficient reaction brightness (>235000 lux). The square container was placed under the ultraviolet lamp for 5min. The sample with different patterns and scales can be obtained by putting the mask plates on container. Finally, the square container with the SPBSS was taken out, and the SPBSS can be taken after cooled at ambient temperature. The SPBSS can be cut as required as possible.

Preparation of the SEBS fiber film

First, SEBS was dispersed in THF at a ratio of 1:7 and stirred for 1 h at ambient temperature. Then, the solution was loaded into a 1 mL syringe with a needle. During electrospinning, the injection speed of the solution was kept at a value of 2.0 mL h^{-1} and positive 12KV voltage was applied to the needle. The SEBS fiber film was collected using a metal plate which was applied negative 5KV voltage.

Characterization

The stress analysis and electric field distribution of SPBSS was described and calculated by COMSL Multiphysics 6.0 (Physical Simulation, Sweden). Mechanical strain tests were conducted using a flexible electronics tester (Shanghai Prtronic Co., Ltd, China) and an electrochemical workstation (shanghai CH Instruments Co., Ltd, China). The loading and unloading rate were set to 60 mm min^{-1} and the apply voltage was set to 0.1 V during strain-R_{rc} test. The loading and unloading rate were set to 15.7 mm min^{-1} and the apply voltage was set to 0.1 V during cyclic stretch fatigue tests. The microscopic morphologies of the SPBSS were examined using a field emission scanning electron microscope and Energy-dispersive X-ray spectroscopy (EDS) (FE-SEM, LEO-1530, Zeiss, Germany). The thickness and the scale of silver-nanoparticle was obtained by analyzing surface of SPBSS in the SEM images using ImageJ software (Media Cybernetics, USA). The observation of the SPBSS with different strain was presented using an optical microscope (Olympus Co., Ltd, Japan). X-ray diffraction (XRD) patterns from the samples were recorded with an X-ray diffractometer (D/max-

2500/PC, Rigaku, Japan) equipped with Cu Kα radiation (λ = 1.54178 Å) with 2θ ranging from 10° to 90°. The elemental composition of the SPBSS was analyzed with an X-ray photoelectron spectrometer (XPS, Escalab Xi+, Thermo Fisher, USA) equipped with an Al Kα excitation source. Mechanics test was carried out by a microcomputer controlled electronic universal testing machine (C42.503, China). Sheet resistance of SPBSS is measured by a sheet resistance tester (HPS2524, China). The multi-channel signal acquisition was calculated and recorded by Arduino platform, and the Interface Controller & CPU was ATmega328.

Micromorphological and chemical analysis

XPS analysis of the products after reaction can provide information on the elements and chemical bonds of the final products. As show in Fig. S9, the fitting results of the characteristic peaks of XPS excited by the Ag3d orbitals give two characteristic peaks which is a typical gap of 6 eV for metallic silver[1]. In the fitting results of C1s XPS characteristic peaks, binding energy 284.8eV, 286.6 eV and 285.9 eV show C-C, C-C and C-N characteristic peak of functional group vibration which prove the sample of SPBSS still existence PAN framework[2].

Model fitting and simulation

Island-bridge model

In island-bridge model (Fig. 2d), R_1 is a constant and R_c is proportional to strain. At high strain situation we got $R_2 \gg R_1$ and R_c, therefore, equation (3) can be re-written as below:

$$R = 2R_1 + R_c \qquad (S1)$$

where R_1 is found to be 3.775 Ω according to experimental data, and $R_c(\Omega) = 30.77(\Omega/\%) \times strain(\%)$.

Optical microscopy experiment

After shaping the sample, fix it in the 3D printed mold. The size of the sample in test is 22mm * 10mm, and the 3D printed mold has a scale with the accuracy of 0.5mm. The stretching mold and sample was placed under the optical microscope, and mark a certain area in surface with a marking pen. Take the optical image of marking area in the unstretched state through the optical microscope. And then take out the mold, stretch the sample which the distance of each stretch is 1mm. Repeat the operation and take the optical images of different strain.

Simulation on COMSOL Multiphysics

All simulations on COMSOL Multiphysics were performed on steady-state. For stress concentration effect simulation, the model was set as a cube (1.00*0.80*0.50 mm) with two narrow grooves (0.02*0.60*0.50 mm) respectively on 1/3 and 2/3 of the long side (x-axis) (Supplementary Fig. S1). Material of the model was set as Skin. Two boundary conditions of solid mechanics interface include fixed constraint and prescribed displacement were respectively added on two x-y boundary surfaces of the model, forming effective strain from 0.1% to 0.3%. Finally, x-z cross-section colored stress patterns were outputted for stress analysis.

For electric potential and electric field analysis, we built five different model based on optical microscope images of SPBSS on different strain conditions, the model size followed the real size of each sample (Supplementary Fig. S11). Material of the model was set as metallic silver with a thickness of 7 μm. Three hypothetical equations were included in this steady-state research:

$$\nabla \cdot J = Q_{j,V} \quad (S2)$$

$$J = \sigma E + J_e \quad (S3)$$

$$E = -\nabla V \quad (S4)$$

In this section, 0.1 V terminal electric potential (U_T) was applied between two y-z boundary surfaces, terminal current (I_T), electric potential and field distribution on x-y surface for each model were outputted and analyzed.

Triangulation location

For triangulation location, three SPBSS are placed on the vertexes of an equilateral triangle with a distance of L. As mentioned in main text, R_{rc} of SPBSS decays exponentially with the distance from vibration source as equation (5) according to one-dimensional vibration experiment, wherein, fitting parameters A and β are 18.72 and 4.32, respectively. Therefore, the equation can be re-written as equation (7):

$$r_N = -4.32 \ln \frac{R_{rc}(N)}{18.72}, (N = 1,2,3)$$

To describe the source location, we established three circle equations with sensors S1, S2 and S3 as the center of the circles:

$$x^2 + y^2 = r_1^2 \quad (S5)$$

$$(x - L)^2 + y^2 = r_2^2 \quad (S6)$$

$$\left(x - \frac{L}{2}\right)^2 + \left(y - \frac{\sqrt{3}}{2}L\right)^2 = r_3^2 \quad (S7)$$

Obviously, the coordinate of vibration source, V(x, y), are the solutions to the equation (S5) to equation (S7), thus we can derive equation (6).

Human-machine interfaces

Neutral layer law

During the bending process of the material, the outer layer is stretched and the inner layer is squeezed. There must be a transition layer on its section that is neither tensile nor compressive. The stress is almost zero. This transition layer is called the neutral layer of the material. The length of the neutral layer during bending is the same as that before bending, and remains unchanged. The neutral layer is the basis for calculating the developed length of bent parts.

As shown in the Supplementary Fig. S19, when the sample is bending, the length of the neutral layer remains unchanged. Where l, $l^{'}$, h, θ, R and $\frac{1}{2}h$ are the length of sample with unloading, the length of sample with bending, the thickness of sample, bending angle, bending radius and the thickness of neutral layer.

$$l^{'} = 2\pi R * \frac{\theta}{360^{\circ}} \qquad (S8)$$

$$l = 2\pi\left(R - \frac{1}{2}h\right) * \frac{\theta}{360^{\circ}} \qquad (S9)$$

$$\Delta l = l^{'} - l = h\pi * \frac{\theta}{360^{\circ}} \qquad (S10)$$

According to the formula we deduce, the strain of sample with bending $\Delta l = h\pi * \frac{\theta}{360^{\circ}}$, which mean there is a linear relationship between bending angle and strain.

Fabrication of electrical glove

General medical rubber gloves were combined with sensor. Sensor fixed at the position corresponding to the second joint of the human finger, and the thumb at the only joint. Connect the silver-plated wire with both ends of the sensor through insulating tape and fix it on the rubber gloves.

Signal acquisition

Arduino platform was used to design the schematic diagram of signal acquisition and transmission circuit. Arduino is a convenient and powerful electronic prototype platform with functional output/input (I/O) pins, which can measure the resistance change of the sensor according to the schematic diagram. The sensor signal acquisition circuit were designed according to different experiments is shown in Fig. S16 and S17. For the resistance measurement of the sensor, the partial voltage resistance measurement method was adopted, that is a known resistance is connected in series on the sensor to be measured to give a known voltage to the circuit, and the voltage value at both ends of the sensor is measured through the (I/O) pin of Arduino chip. The resistance of the sensor is calculated by the partial voltage formula. If it is necessary to collect and save the sensing signal, the information can be transmitted to the computer through serial communication.

Signal mapping and Bluetooth transmission

In LED matrix control test, real-time resistance (R_{rt}) was measured and calculated by Arduino platform (Fig. S16), and R_{rc} calculated by R_{rt} was divided in three regions. Each region corresponds to a LED matrix display combination of English letter. Under the corresponding R_{rc} condition, the content display of LED is controlled by program.

In the Bluetooth car control experiment, the Arduino measurement channel were expanded to 4 and connected the Bluetooth module on Arduino. Each measurement channel corresponds to a separate sensor (Fig. S17 and S18). The R_{rt} of each sensor is measured separately and the corresponding R_{rc} is calculated. The R_{rc} corresponding to each sensor represents an action of the Bluetooth car, namely "Forward", "Backward", " Turn right" and " Turn left ". When the R_{rc} corresponding to the sensor exceeds the threshold set in the program, the Bluetooth module connected to Arduino transmits the corresponding instructions to the Bluetooth car, and the Bluetooth car takes corresponding actions after receiving the corresponding instructions. When the Bluetooth car receives different commands at the same time, for example, the "forward" and "backward" commands appear at the same time, its operation is carried out in the order of "Forward", "Backward", " Turn right" and " Turn left ".

Recognition of steady-state gestures

In the steady-state gestures (SSGs) recognition experiment, the number of acquisition channels were increased to five which is the number of one hand, and collected ten different sets of gesture signal data, including the individual bending data of each finger and some simple gesture language. These gesture data well reflect the characteristics of gesture images, that is, bending fingers have high signal intensity. For the traditional classification model, it is difficult to effectively classify the gesture data, especially when there are multiple objects. In order to effectively and accurately classify and recognize these gesture data, we introduced a machine learning library

(Scikit-learn), which has various classification, regression and clustering algorithms for training gesture recognition[3].

The whole SSGs recognition is divided into two parts: training and translation. In training section, SSGs data were collected by wearable devices. Before feeding SSGs data into Scikit-learn training, the signals must be processed. Pandas was used to input SSGs data as array which was merged into a set X. And then the set X was converted $x_i \in R^{40 \times 5}$ from 2-dimensional to 1-dimensional data $x_i \in R^{800}$. The set X was split to get the training set and test set. Using the LogisticsRegression API $LogisticRegression.fit(x,y)$ to train the training set. Finally, the classification prediction model $LogisticRegression.predict(x)$ was used to display the classification results and checked the accuracy rate to evaluate the model.

Recognition of dynamic gestures

The data of DGs recognition was collected continuously, we take 4 seconds as an action interval, which mean the subject only act one dynamic gesture in four seconds and doing nothing expect the gesture. In the experiment, we distinguish each gesture by adding a rest character to dataset. Rest character not only ensure that each group of gesture data has same data points which ensure the uniformity of data, but also giving the coordinates of the data time variable. In addition, the DGs set also show that even one subject doing the same gesture, the data of the five fingers intensity still have huge different and that's reason we use deep learning to train the model which can recognize the gesture by these data.

Significantly, a new variable time is introduced in DGs recognition. DGs data was described as continuous data points on the time axis. Traditional mechanical learning models like Scikit-learn use K Nearest Neighbor (KNN) algorithm. In KNN algorithm if most of the k most similar samples in the feature space (that is, the closest samples in the feature space) belong to a certain category, the sample also belongs to this category[4, 5]. The distance between two samples can be expressed by Euclidean distance, and the distance formula between point a (x_{11}, x_{12}, ...x_{1n}) and point b (x_{21}, x_{22}, ...x_{2n}) in N-dimensional space is as follows:

$$d_{12} = \sqrt{\sum_{k=1}^{n} (x_{1k} - x_{2k})^2} \qquad (S11)$$

KNN machine learning algorithm is mature in theory and simple in thought. It can be used for classification and regression as well as nonlinear classification. However, it is worth noting that the training time complexity of KNN is lower than that of support vector machine (SVM) algorithm which mean KNN can't handle time-related variables well. And when the number of features is very large, the calculation will increase.

To solve the defects of KNN algorithm, we introduced Vision Transformer (ViT) as the training model. Compared with KNN algorithm, ViT uses the self-attention mechanism to make the model parallel training and master the global information[6-9]. In ViT, Multi-Layer Perceptron (MLP) solves the flaw of traditional mechanical learning models. MLP splits the data in a data group into patches, and then uses linear projection to convert each patch into a vector, which maps the block into a vector space. These vectors are coupled with information about the location of patches in the dataset and submitted to the classic transformer. Finally, perform self-attention on the data and generate the results, and perform different downstream tasks according to the results.

Compared with KNN algorithm, ViT achieves excellent results with variable of time and requires less data for training.

In DGs recognition, the data of dynamic gesture combined with the GesViT to train which include MLP to cross validation. Ten dynamic gestures represent different meaning in sign language and these data with different intensity characteristics constitute the data set required for GesViT, which is used as training data for dynamic gesture recognition. Similar to SSGs recognition, DGs set was also split into training set and test set. After training with GesViT, the dynamic gesture recognition prediction model which was trained by deep learning shows high accuracy. The predicted results returned after MLP head training can be seen that the prediction results show high accuracy and relevance after training. F1-score of the model shows the high accuracy of dynamic gesture recognition after machine learning. F1-score is an evaluation index used for classification model in machine learning, including precision and recall which F1 score is their average value.

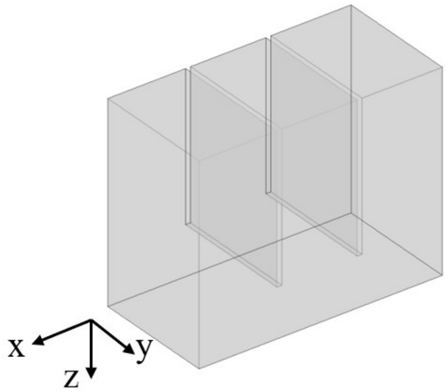

Fig. S1 3D model of crack structure for stress concentration effect.

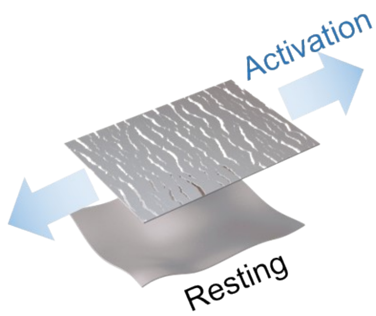

Fig. S2 Schematic of biomimetic sensor with silver nanoparticle functional layer and a flexible polymer substrate.

Fig. S3 Luminous intensity of the UV source.

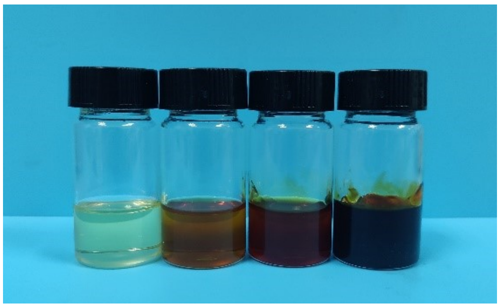

Fig. S4 Optical image of precursor solutions which changed with time.

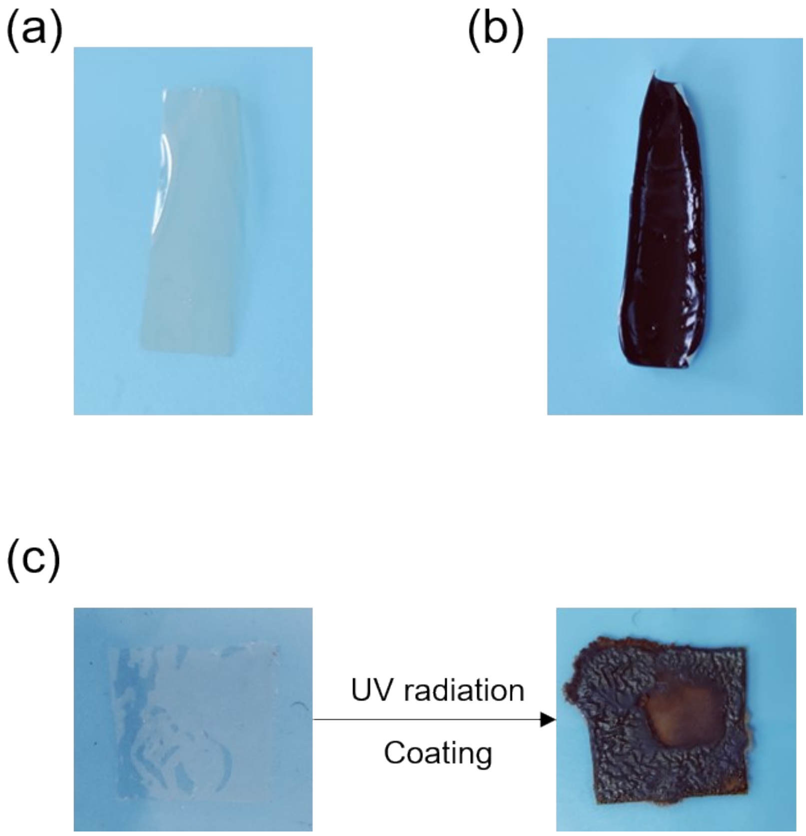

Fig. S5 (a) Optical image of PAN film. (b) Optical image of PAN complexes. (c) Optical image of PAN film after coating silver nitrate and UV radiation.

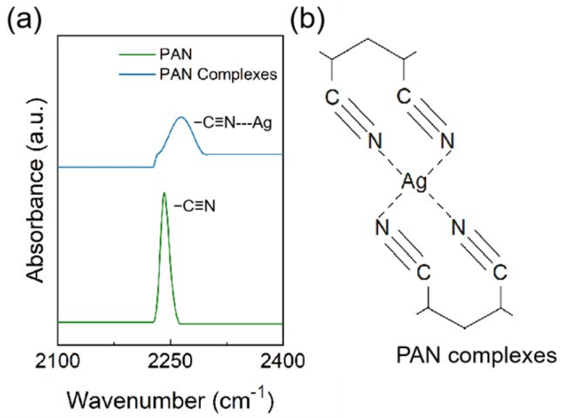

Fig. S6 (a) FTIR spectra of PAN and PAN Complexes, showing different chemical environments of nitrile groups. (b) the schematic for the primary molecular interactions within PAN complexes network.

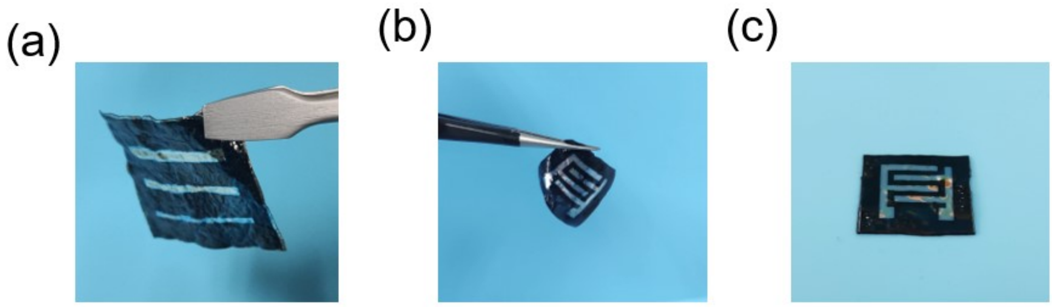

Fig. S7 Optical image of SPBSS with different patterns. (a) Optical image of SPBSS with different line wires widths. (b) Optical image of SPBSS with interdigitated structure showing flexibility. (c) Overhead angle optical image of SPBSS with interdigitated structure.

Fig. S8 Optical image of as-prepared SPBSS which were cut into geometric figures ("circular", "square", "triangle") and letters ("G", "X", "U").

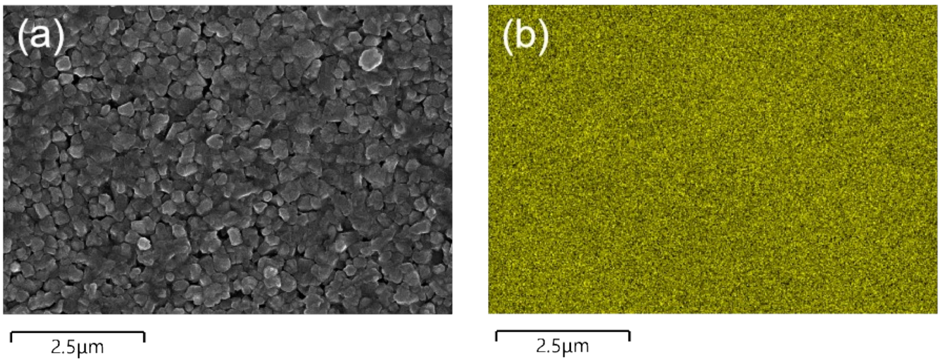

Fig. S9 (a) SEM image of SPBSS with AgNPs on the surface, (b) and corresponding element mapping of silver.

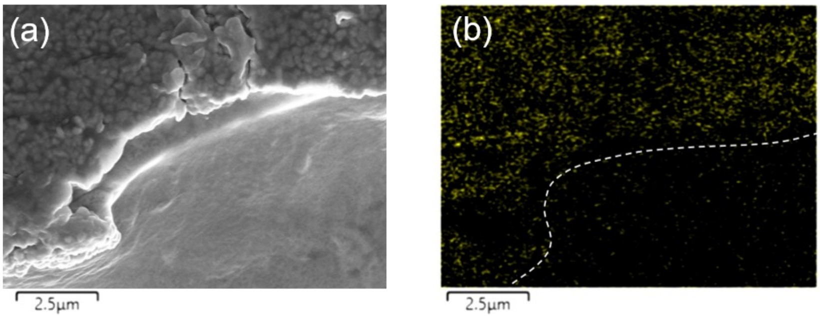

Fig. S10 (a) Cross-section SEM image of SPBSS with double-layer structure consists of a uniform electrical conductive AgNPs top layer, and corresponding elements mapping of (b) silver.

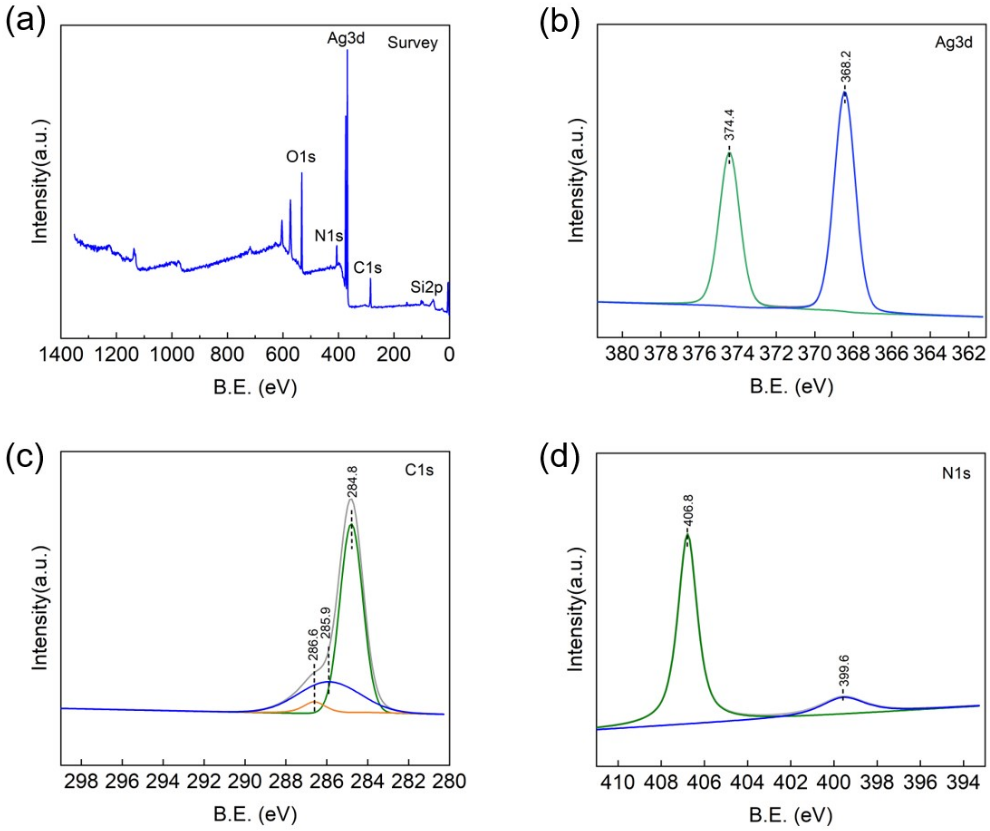

Fig. S11 XPS spectrum of SPBSS. (a) XPS spectrum of SPBSS for all elements. (b) High resolution XPS spectrum of SPBSS for Ag elements. (c) High resolution XPS spectrum of SPBSS for C elements. (d) High resolution XPS spectrum of SPBSS for N elements.

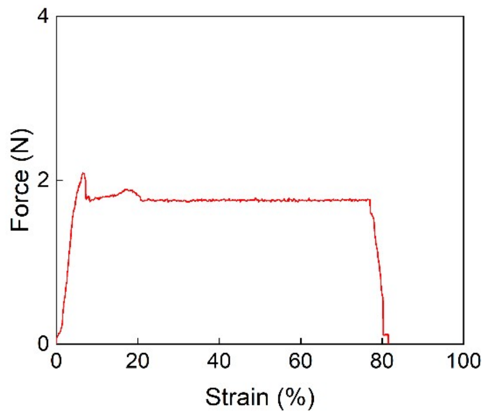

Fig. S12 Force-strain curves of SPBSS was stretched until fracture.

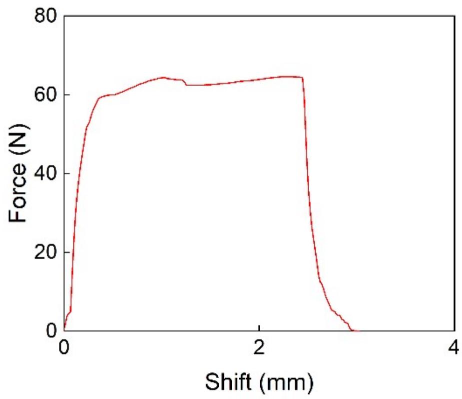

Fig. S13 Force-Shift curves of SPBSS which AgNPs were stripped from PAN substrate until fractures.

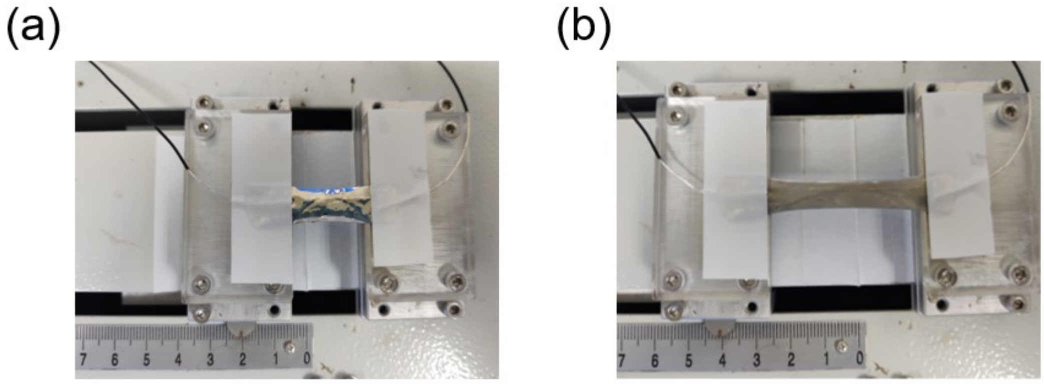

Fig. S14 Optical image of SPBSS with different strained state. (a) Optical image of SPBSS with unstretched state. (b) Optical image of SPBSS with 100% strain state.

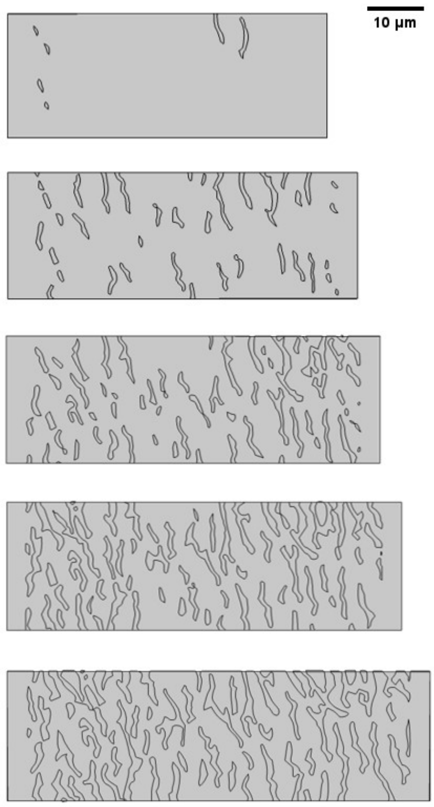

Fig. S15 Schematic of SPBSS with microcrack structure under different strain of 0%, 4.5%, 9.0%, 13.6% and 18.2%.

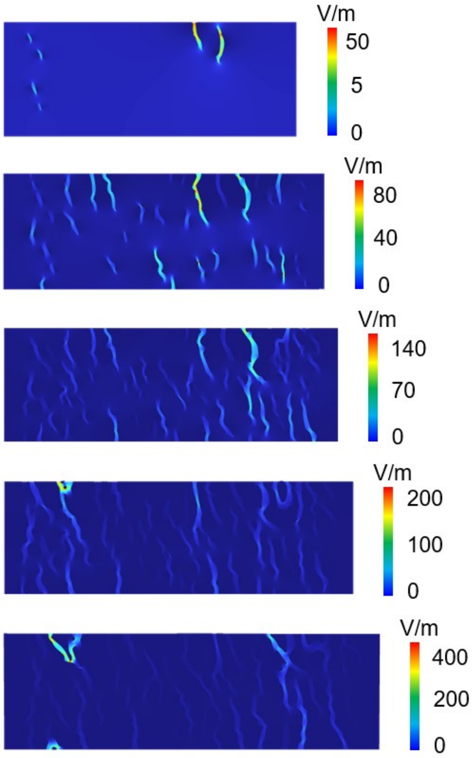

Fig. S16 Potential distribution of the SPBSS under different strain of 0%, 4.5%, 9.0%, 13.6% and 18.2%.

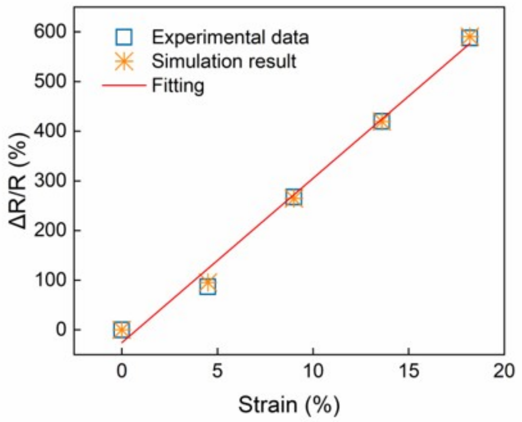

Fig. S17 R_{rc}-strain curves of simulation results which fitting from experimental data show good linearity.

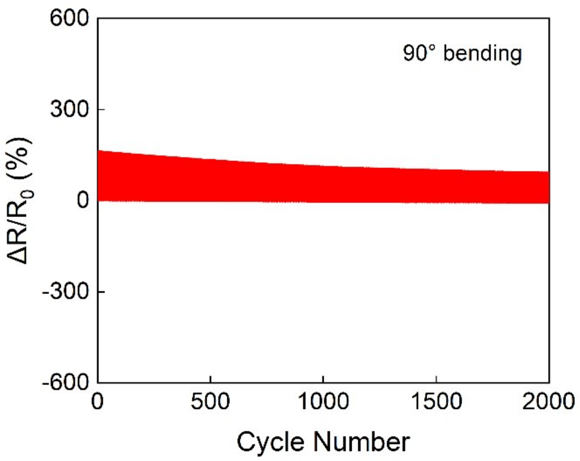

2 **Fig. S18** RCR-strain curves of SPBSS at 90 degrees for 2000 numbers of cycles.

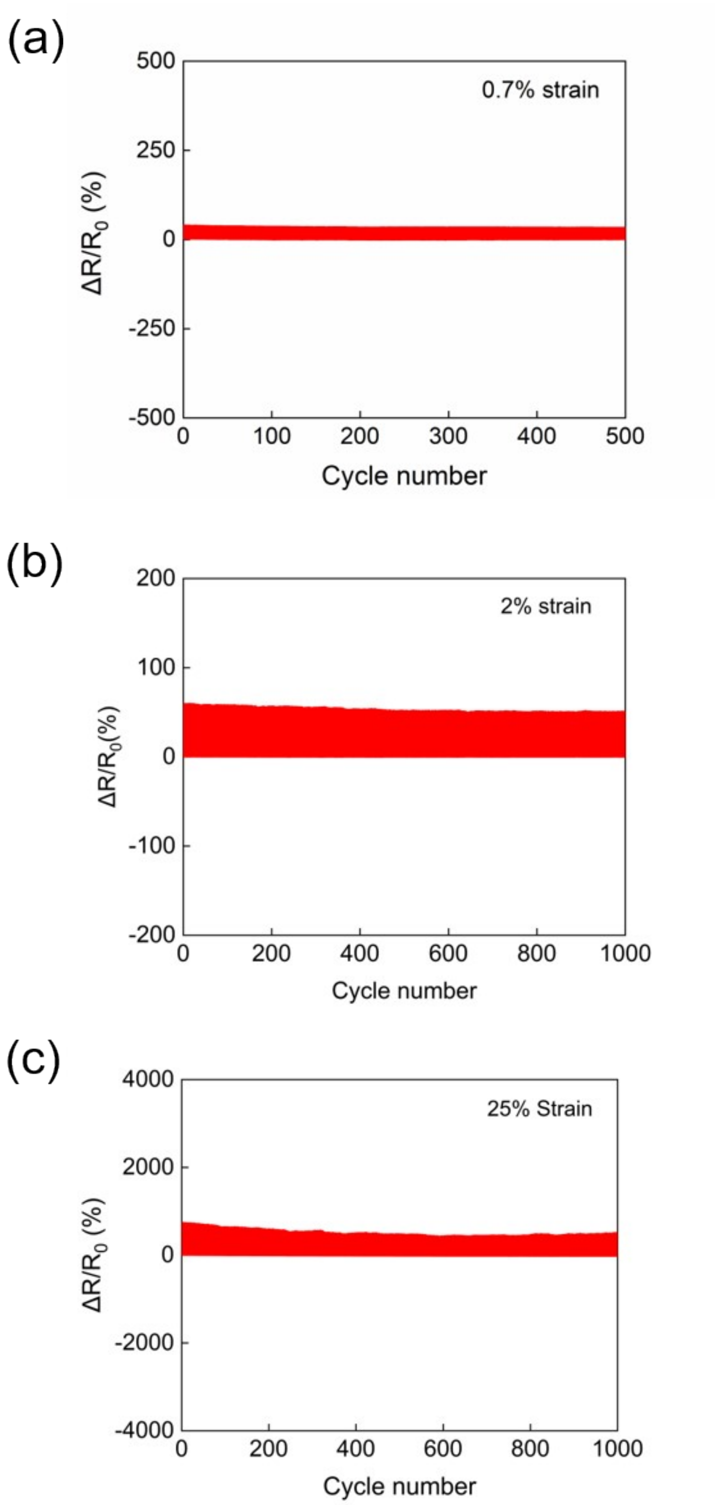

Fig. S19 Mechanical fatigue test of SPBSS. (a) RCR-strain curves of SPBSS at 0.7% strain for 500 numbers of cycles. (b) RCR-strain curves of SPBSS at 2% strain for 1000 numbers of cycles. (c) RCR-strain curves of SPBSS at 25% strain for 1000 numbers of cycles.

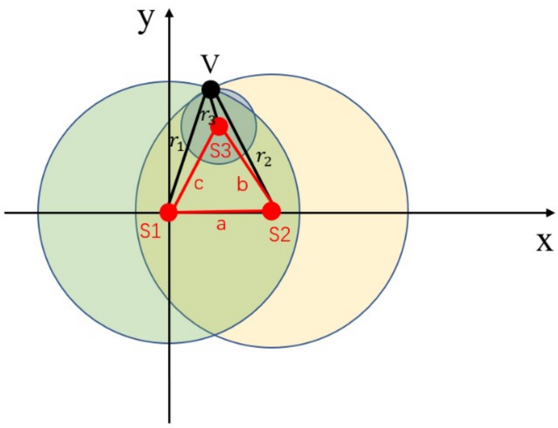

Fig. S20 Schematic diagram of triangulation in cartesian coordinate system.

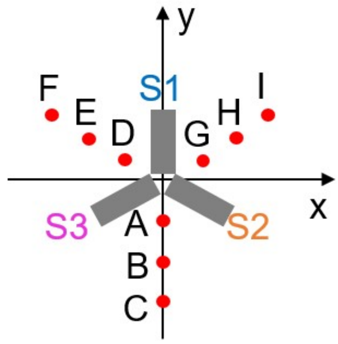

Fig. S21 Rectangular coordinate system of vibration detection with position of vibration and SPBSS.

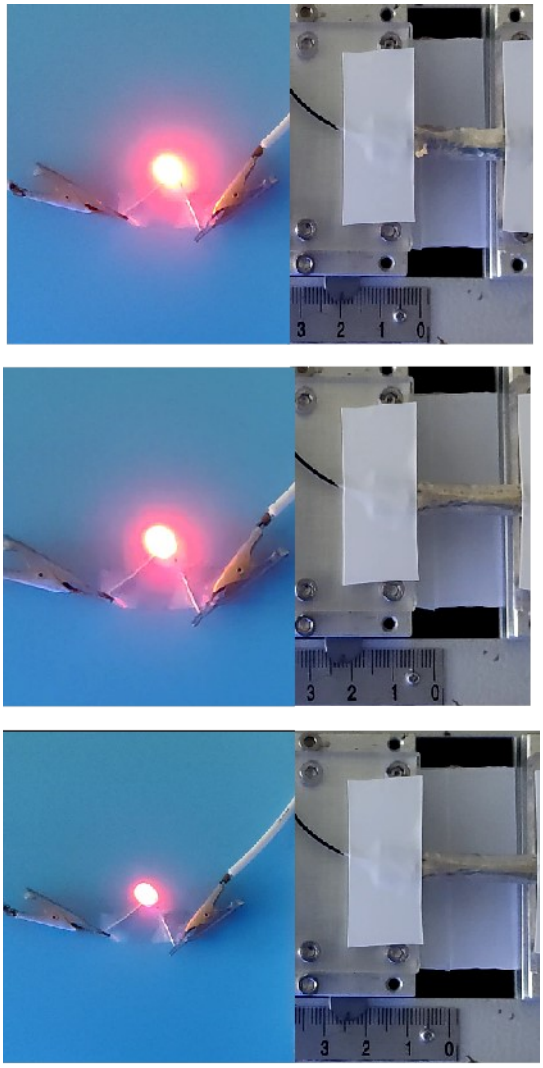

Fig. S22 Optical image of LED connected series with SPBSS under 0%, 10%, and 25% strain.

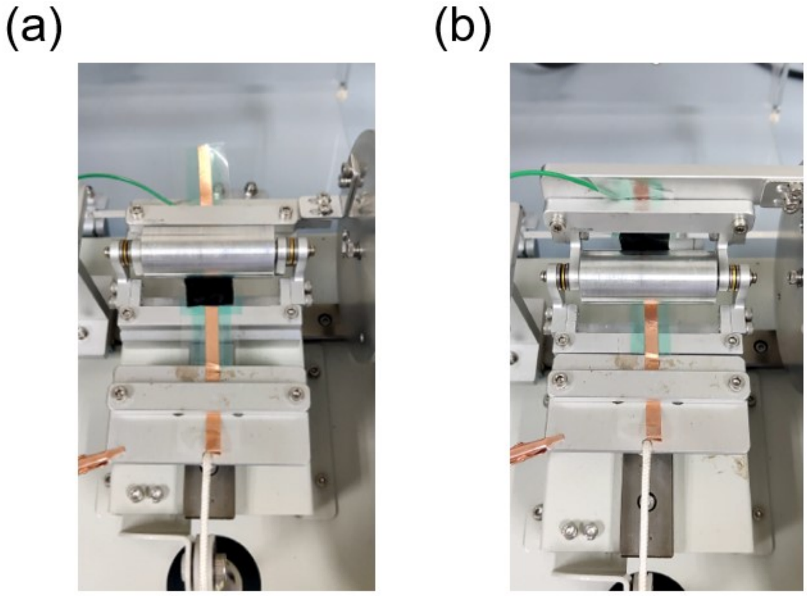

Fig. S23 Optical image of SPBSS in bending test. (a) Optical image of SPBSS under unbending state. (b) Optical image of SPBSS under 90°bending.

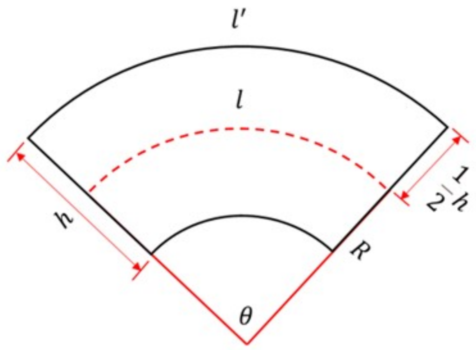

Fig. S24 Schematic showing sample in bending state with neutral layer.

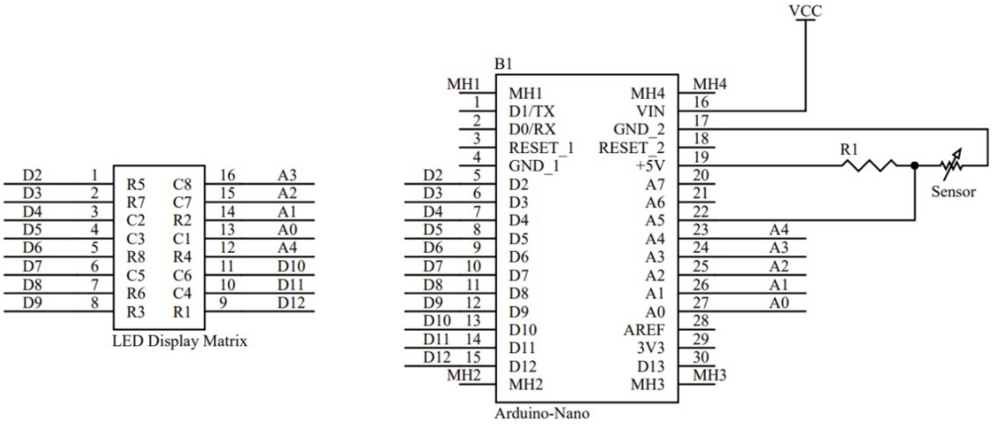

Fig. S25 The circuit schematic diagram of Arduino-Nano with resistance measurement and LED display matrix modular.

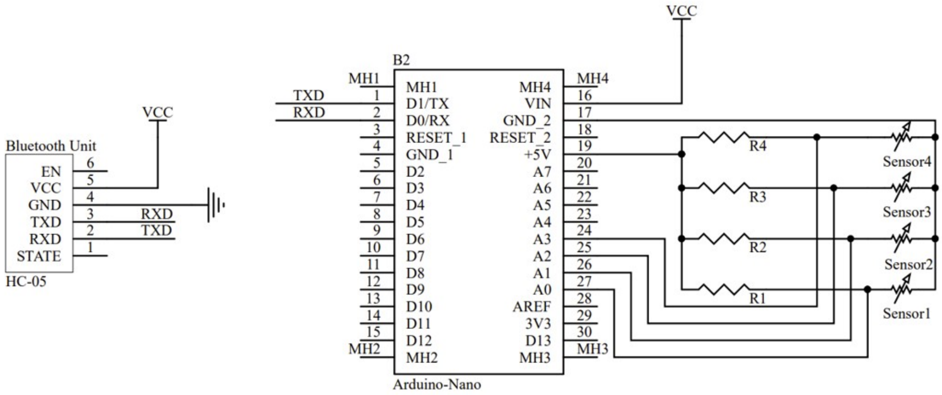

Fig. S26 The circuit schematic diagram of Arduino-Nano with 4 channels resistance measurement and Bluetooth module.

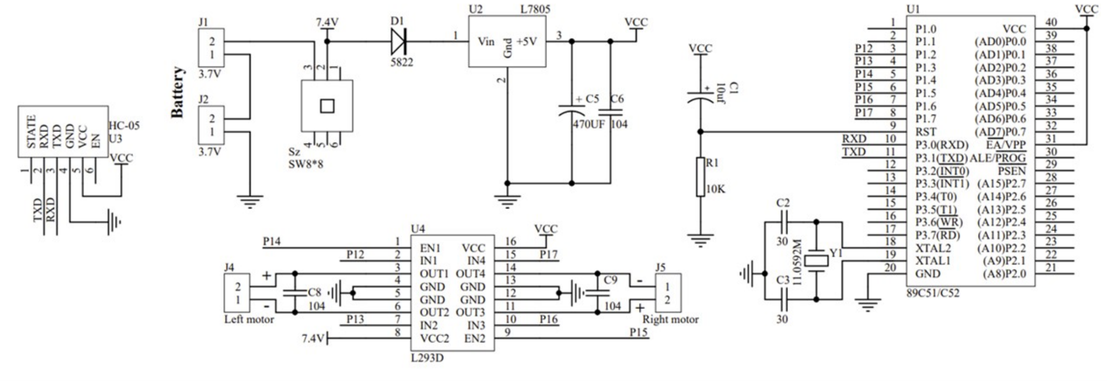

Fig. S27 The circuit schematic diagram of the mini Bluetooth car.

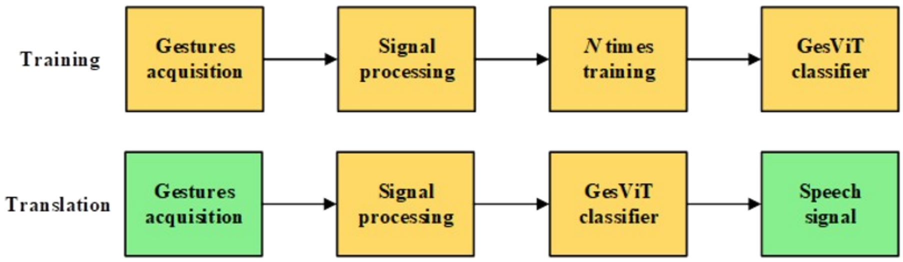

Fig. S28 The flow-process diagram of ViT in training and translation.

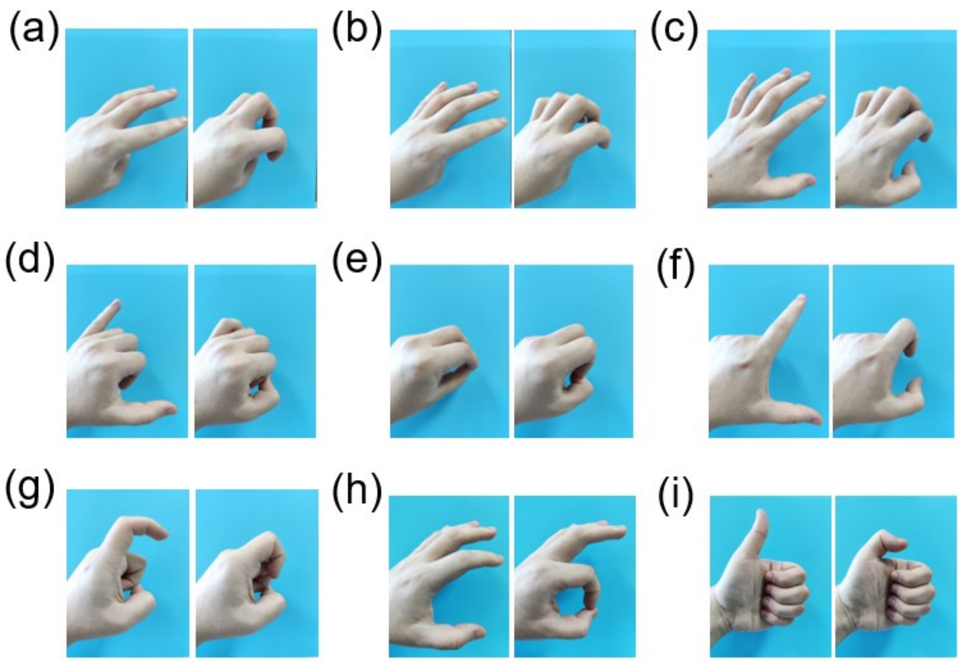

Fig. S29 Optical images of dynamic gestures represent “30”, “40, “50”, “60”, “70”, “80”, “90”, “Money”, “Thanks” separately.

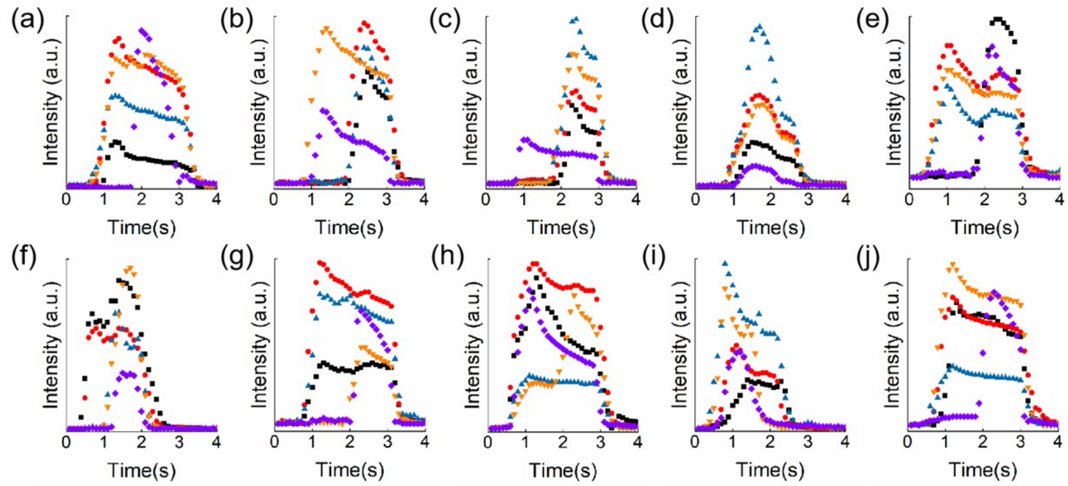

Fig. S30 Intensity distribution of dynamic gestures in 4 seconds represent “30”, “40, “50”, “60”, “70”, “80”, “90”, “Money”, “Thanks” separately.

Table S1. Fabrication time of SPBSS and other strain sensors.

Strain Sensor	Time of Fabrication	Time of Precursor Solution	Total Time	References
This work	5 min	3 hours	3 hours and 5 min	--
PEDOT/Fabric	3 hours and 30 min	30 min	4 hours	Ref.33
Carbonized Crepe Paper/PDMS	10 hours and 20 min	--	10 hours and 20min	Ref.7
CNT/Ni foam	13 hours	2 hours	15 hours	Ref.38
MWNTs/PDMS	24 hours	--	24 hours	Ref.40
MXene/Cellulose Nanocrystal	14 hours and 40 min	24 hours and 30 min	39 hours and 10 min	Ref.12
Carbon Paper/PDMS	5 hours and 40 min	--	5 hours and 40 min	Ref.41
NR/ChNCs-CB composite	4 hours	6 hours and 20 min	10 hours and 20min	Ref.16
Carbon Black/PDMS	4 hours	--	4 hours	Ref.6
Ni foam/Graphene/PDMS	21 hours	--	21 hours	Ref.42
DN-FT-HCl hydrogel	18 hours	6 hours	24 hours	Ref.3
Carbon Black/TPU	5 hours and 30 min	4 hours	9 hours and 30 min	Ref.43
Conductive Polymer Composites/PU	10 hours and 20 min	30 min	10 hours and 50min	Ref.22
CNT/MXene/PDMS	5 hours	2 hours	7 hours	Ref.26

Supplementary Video S1. A SPBSS controlled LED matrix for controllable content display.

Supplementary Video S2. Basic driving commands (forward, backward, turn right, and turn left) of a mini Bluetooth car controlled by SPBSS electronic gloves.

Supplementary Video S3. Continuous obstacle avoidance of the mini Bluetooth car controlled by SPBSS electronic gloves.

Supplementary References

1 V. K. J. J. o. E. S. Kaushik and R. Phenomena, *J. Electron Spectros. Relat. Phenomena*, 1991, **56**, 273-277.

2 C. R. Wu, W. R. Salaneck, J. J. Ritsko and J. L. Bredas, *Synth. Met.*, 1986, **16**, 147-159.

3 F. Pedregosa, G. Varoquaux, A. Gramfort, V. Michel, B. Thirion, O. Grisel, M. Blondel, P. Prettenhofer, R. Weiss and V. J. t. J. o. m. L. r. Dubourg, 2011, **12**, 2825-2830.

4 S. Zhang, X. Li, M. Zong, X. Zhu and D. Cheng, *ACM Transactions on Intelligent Systems and Technology*, 2017, **8**, 1-19.

5 G. Guo, H. Wang, D. Bell, Y. Bi and K. Greer, Berlin, Heidelberg, 2003.

6 A. Dosovitskiy, L. Beyer, A. Kolesnikov, D. Weissenborn, X. Zhai, T. Unterthiner, M. Dehghani, M. Minderer, G. Heigold and S. J. a. p. a. Gelly, *arXiv preprint arXiv:2010. 11929.*, 2020, 11929.

7 A. Steiner, A. Kolesnikov, X. Zhai, R. Wightman, J. Uszkoreit and L. J. a. p. a.

Beyer, *arXiv preprint arXiv:2106. 10270.*, 2021, 10270.

8 I. O. Tolstikhin, N. Houlsby, A. Kolesnikov, L. Beyer, X. Zhai, T. Unterthiner, J. Yung, A. Steiner, D. Keysers and J. J. A. i. n. i. p. s. Uszkoreit, *Advances in neural information processing systems*, 2021, **34**, 24261-24272.

9 A. Vaswani, N. Shazeer, N. Parmar, J. Uszkoreit, L. Jones, A. N. Gomez, Ł. Kaiser and I. J. A. i. n. i. p. s. Polosukhin, *Advances in neural information processing systems*, 2017, **30**, 30.